Acta Materialia 103 (2016) 483–494

Contents lists available at ScienceDirect

Acta Materialia

journal homepage: www.elsevier.com/locate/actamat

Full length article

# Temperature-dependent size effects on the strength of Ta and W micropillars

Oscar Torrents Abad [a,b], Jeffrey M. Wheeler [c,1], Johann Michler [c], Andreas S. Schneider [a,2], Eduard Arzt [a,b,*]

[a] INM – Leibniz Institute for New Materials, Campus D2 2, 66123, Saarbrücken, Germany
[b] Department of Materials Science and Engineering, Saarland University, 66123, Saarbrücken, Germany
[c] Empa – Swiss Federal Laboratories for Materials Science and Technology, Laboratory for Mechanics of Materials and Nanostructures, Feuerwerkerstrasse 39, 3602, Thun, Switzerland

ARTICLE INFO

*Article history:*
Received 17 July 2015
Received in revised form 30 September 2015
Accepted 9 October 2015
Available online 6 November 2015

*Keywords:*
Crystal plasticity
Compression test
Micropillar
Size effect

ABSTRACT

The strength of metals increases with decreasing sample size, a trend known as the size effect. In particular, focused ion beam-milled body-centered cubic (BCC) micropillars exhibit a size effect known to scale with the ratio of the test temperature to the critical temperature ($T_c$) of the BCC metal, a measure of how much the yield stress is governed by the lattice resistance. In this paper, this effect is systematically studied by performing high-temperature compression tests on focused ion beam-manufactured Ta and W single crystal pillars ranging in diameter from 500 nm to 5 μm at temperatures up to 400 °C, and discussed in the context of bulk strength and size dependent stresses. Both metals show larger size effects at higher temperatures, reaching values that are in the range of FCC metals at temperatures near $T_c$. However, it is demonstrated that size effects can be considerably affected by material parameters such as dislocation density and lattice friction, as well as by the yield criterion used. Furthermore, for W, a change from uniform wavy deformation to localized deformation is observed with increasing temperature and pillar size, further indicating that the temperature ratio strongly influences the relative motion of screw and edge dislocations.



## 1. Introduction

The mechanical properties of submicron and micron-sized structures differ from those of bulk material. When the dimensions of a sample are similar to or smaller than the microstructural length scales, interfaces and free surfaces become important. In particular, such 'size effects' have been observed for metals, where the strength usually increases with decreasing sample size. The 'dimensional constraint' on dislocation processes then overrides the 'microstructural constraints' that usually dictate the strength in bulk metals [1], or 'external size effects' dominate over 'internal effects' [2]. Researchers have described such size effects by relating mechanical properties and a geometrical or microstructural size scale of interest as follows:

$$\sigma_y = \sigma_0 + kd^n, \quad (1)$$

where $\sigma_y$ is the yield strength of the structure, $\sigma_0$ is the bulk strength of the material, $d$ is the characteristic length scale, and $k$ and $n$ are constants. For example, the Hall–Petch relationship predicts a power-law exponent $n$ of –0.5 for metallic materials in which $d$ is the grain size [3,4]. Thin film tests and compression tests on micropillars have shown typical values for $n$ in the order of –0.5 to –1, where $d$ is the film thickness or pillar diameter. When strain gradients are present, size effects can emerge naturally ('strain gradient plasticity') [5–7], an effect that is ruled out for micropillar compression testing.

Micropillar compression studies have mostly focused on metals with the face-centered cubic (FCC) crystal structure (Ni [8–11], Au [12–17], Cu [18,19] and Al [20]) and the body-centered cubic (BCC) crystal structure (W [21–24], Mo [15,16,21–23,25–28], Nb [22–24,29,30], V [31] and Ta [22,32]). These experiments have reported that, for pillars with diameters ranging from 200 nm to a few micrometers, an inverse power-law relation between yield strength and sample size is observed. For FCC metals, in which the bulk strength, $\sigma_0$, is usually negligible, the power-law exponent, $n$, lies in the range of –0.6 to –1.0 [2,10,11,13,14,18,20,33–36]. On the

* Corresponding author.
*E-mail address:* eduard.arzt@leibniz-inm.de (E. Arzt).
[1] Present address: ETH Zürich, Department of Materials, Laboratory for Nanometallurgy, Vladimir-Prelog-Weg 1-5/10, 8093 Zurich, Switzerland.
[2] Present address: AG der Dillinger Hüttenwerke, P.O. Box 1580, 66763 Dillingen/Saar, Germany.

http://dx.doi.org/10.1016/j.actamat.2015.10.016

contrary, BCC metals have shown a weaker size dependence than FCC metals; their behavior was found to correlate with their critical temperature that signifies the transition from a strong to a weak temperature dependence of the flow stress in BCC metals [22]. The different degrees of size dependence have been attributed to different contributions of the lattice resistance to plastic strength of each particular BCC metal (which is dependent on the Peierls potential of the metal and is independent of size) [15,22]. Unlike in FCC metals, screw dislocations in BCC metals have a rather complex non-planar core structure with a threefold symmetry [37]. Consequently, BCC metals present high Peierls potentials that lead to low mobility of the screw dislocations in comparison to edge dislocations [38]. As the ratio of the test temperature to the critical temperature ($T_c$) was found to correlate with the magnitude of the size dependence, it was proposed that the decreasing size dependence in BCC micropillars reflects the decreasing mobility of the screw dislocations [21,22]. However, size effects in BCC metals have been typically determined without considering the contribution of bulk stresses, $\sigma_0$, which are often in the order of hundreds of MPa for BCC metals at room temperature and should not be neglected [32,39–41].

Different studies have tried to understand the role of bulk stresses, more precisely the role of the lattice resistance on the size effect of micropillars [21,39,42]. Lee and Nix [42] have carefully compared the power-law exponents of focused ion beam (FIB) machined FCC and BCC micropillars by considering different material parameters. Material parameters such as lattice friction, dislocation density, shear modulus and Burgers' vector, which are size independent but can depend on temperature, affect the size dependence in submicron and micron-sized pillars [21,42–45]. Lee and Nix suggested that the main argument for the different power-law exponents is the value of lattice friction, and this was rationalized in terms of the single-arm dislocation source model first proposed by Parthasarathy et al. [46]. At a moderate dislocation density ($10^{12}$–$10^{13}$ $m^{-2}$), the strength of micropillars with diameters of a few micrometers was assumed to be controlled by the operation of single-arm dislocation sources, which are Frank-Read sources truncated at the free surface [42,45]. Through this model, the critical resolved shear stress of a pillar with a diameter of a few micrometers can be calculated as the linear superposition of the lattice resistance in shear, $\tau_0$, a work-hardening term containing the total dislocation density, $\rho_{tot}$, and a size-dependent term:

$$\tau_{CRSS} = \tau_0 + 0.5\mu b\sqrt{\rho_{tot}} + \frac{\alpha\mu b}{\bar{\lambda}_{max}(d, \rho_{tot}, \beta)} \cong \tau_{bulk} + \tau_{size\ dependent}, \quad (2)$$

with the shear modulus $\mu$, the Burgers' vector $b$, the line tension of the weakest single-arm dislocation source determined by the statistical average length of the weakest source $\bar{\lambda}_{max}$, and a geometrical constant of order of unity $\alpha$ [46]. The dependence of the lattice friction on power-law exponents has been recently demonstrated by Soler et al. [47]. Chemically etched LiF micropillars, with a controlled initial dislocation density, were tested at different temperatures and rigorously analyzed by using Parthasarathy's model. The authors concluded that size effects are the result of the relative contributions of bulk stresses and size-dependent stresses. It was shown that at room temperature, bulk stresses dominated the absence of size effect, while at 250 °C, both contributions were of the same order, thus giving rise to a large size effect.

To improve the understanding of the size effect in BCC metals, tests conducted at different relative temperatures (compared to the critical temperature) are required. So far, only two studies have varied this parameter in BCC metal pillars [21,24]: Schneider et al. [21] have shown that Mo micropillars tested at 500 K (above $T_c$ for this materials) exhibit a size dependence very close to that of FCC metals, suggesting that the better mobility of screw dislocations above $T_c$ allowed Mo micropillars to deform as FCC micropillars. As a result, it was suggested that the dislocation process controlling the size dependence in BCC micropillars may be the same as in FCC micropillars: source truncation [46], mechanical annealing [9] and/or dislocation starvation [17]. On the other hand, Lee et al. [24] have recently studied the size dependence of Nb and W nanopillars at 165 K (far below $T_c$ for these materials), and also assessed the stochastic nature of nanopillar deformation together with dislocation dynamics simulations. It was suggested that the surface-controlled dislocation multiplication is restricted when the mobility of screw dislocations is similar to that of edge dislocations, thus resulting in smaller plastic strain bursts at temperatures close to $T_c$ or above. What is lacking so far, however, is a study in which the test temperature is varied systematically.

The aim of the present paper was to investigate the plasticity of BCC pillar structures at the micron and submicron regimes, for the first time, at different temperatures up to 400 °C. Emphasis was placed on Ta and W micropillars. The implications of lattice resistance and dislocation density as well as straining are discussed in the context of size effect dependence on temperature.

## 2. Experimental method

High purity Ta and W single crystals (99.999%) with dimensions of approximately 5 mm × 5 mm × 1 mm were used for this study. The Ta crystal had a [111] and the W crystal a [100] orientation. These orientations were selected to have the same orientations as in previous room temperature studies [22,32]. In addition, two multiple slip orientations were selected to study the influence of orientation on the temperature dependent size effect of BCC metals. The samples were ground with silicon carbide papers down to a grit size of 4000 using a stainless steel cylindrical holder that was employed to produce parallel-sided samples. Subsequently, they were electropolished to reduce the grinding damage and to obtain a flat surface needed for the subsequent microcompression testing. 72 micropillars per sample were FIB manufactured with an FEI Versa 3D DualBeam equipped with a gallium ion source. The pillar milling procedure was carried out in two steps as described by Volkert and Lilleodden [14]: The first step was performed at a beam voltage of 30 kV and beam currents of 7 and 13 nA depending on the pillar dimensions. A second milling procedure, which consisted of multiple steps, was carried out at very low currents, between 10 and 100 pA, to reduce the ion damage and adjust the final pillar shape. The pillars, ranging from 500 nm to 5 μm in diameter with an aspect ratio (length/diameter) of approximately 3, had a taper angle of 2.5 ± 0.4° for the Ta sample and 2.2 ± 0.3° for the W sample.

Compression of the pillars was performed at different temperatures up to 400 °C using an Alemnis indenter at Empa, modified to run at high temperatures inside a Zeiss DSM 962 scanning electron microscope (SEM) [48,49] at a chamber pressure of about $5{\cdot}10^{-5}$ mbar. The indenter was equipped with a diamond flat punch of approximately 9 μm in diameter. The fact that the tests were performed inside the SEM minimized oxidation of the samples at high temperature. The system had two independent thermocouples, one on the indenter tip and another on the sample, such that temperature was accurately controlled. Two different calibrations were made prior to testing: a calibration of the sample-tip temperature difference and a calibration of the compliance of the whole indenter-sample system as described previously by Wheeler and Michler [48]. First, the indenter and sample heaters were set to heat to the desired test temperature so as to reduce the drift produced during testing. Second, a small correction for the compliance of the load frame, as well as another one for the sink-in compliance of the pillars, which rest on the same substrate material, were applied for each test to precisely determine the specific load rate and strain of the

micropillars. The effect of the pillar acting as a flat punch and elastically deforming the substrate during compression as well as the effect of the indenter itself elastically deforming were considered using the Sneddon's solution [14,50].

The Ta micropillars were tested at 25, 100 and 200 °C. On the other hand, W micropillars were compressed at 25, 200 and 400 °C. The tests were conducted under displacement control at fixed displacement rates. The displacement rates were scaled with the pillar height in order to obtain a constant strain rate of $10^{-3}$ $s^{-1}$ for pillars with different heights and a maximum strain of approximately 0.10. The experiments at 25 °C were carried out before those at 100 °C, and the ones at 200 and 400 °C were performed at the end to avoid any possible annealing effect.

To convert the obtained load–displacement data into stress–strain curves, the measured lengths and diameters were used. In view of the tapered pillar shape, the diameter at the top of the pillars was used to determine engineering stress. True stress and true strain were not meant to be determined as the deformation mostly occurred heterogeneously by slip of a few systems. The top diameter was chosen because it is well defined and easy to determine via SEM imaging. Furthermore, the stress is the highest at the top due to the tapered pillar shape. The implications on the determined stress level by choosing an appropriate reference diameter were discussed in detail by Frick et al. [11] and Kiener et al. [36].

## 3. Results

### 3.1. Plastic deformation morphology

Fig. 1 shows SEM images of representative compressed Ta and W micropillars as a function of size and test temperature. Irrespective of pillar diameter and test temperature, all Ta micropillars exhibited slip bands reaching the surface of the pillars as previously reported in the literature [22,32]. Although the [111] is a multiple slip orientation, slip occurred mainly for the preferred slip system and the deformation was localized close to the upper end of the pillars. On the other hand, W micropillars showed traces indicative of multiple slip as observed before [22,24,29]. All W pillars compressed at room temperature exhibited a homogeneous, wavy deformation, indicating cross-slip of screw dislocations. This wavy deformation was also exhibited by small pillars (500 nm in diameter) compressed at higher temperatures. However, larger pillars compressed at higher temperatures showed a transition in deformation mechanism from homogeneous to localized deformation (see Fig. 2). This indicates that a more avalanche dominated behavior caused by the activation of only a few slip systems took place for larger pillars at 200 and 400 °C.

### 3.2. Stress–strain response as a function of pillar size and temperature

Stress–strain curves of representative Ta micropillars compressed at 25, 100 and 200 °C, and W micropillars compressed at 25, 200 and 400 °C are depicted in Figs. 3 and 4, respectively. The distinctive behavior of displacement controlled compression was observed in these curves. Low stiffness artifacts were recorded during first loading as initial contact of the flat punch on pillars took place [14]. Stiffness values then increased and elastic loading started before yield occurred at a critical point. The stress–strain curves of the micropillars with diameters larger than 2 μm were relatively continuous, while, for micropillars between 500 nm and 1 μm diameter, the loading curves showed pronounced stress drops along the whole strain range, indicating that the stress–strain behavior became more stochastic as the diameter of the micropillars decreased. This is in consonance with other experimental studies where such behavior was attributed to the reduction in the number of available dislocation sources as sample size decreased [20,51]. It is readily apparent that the curves for the 500 nm diameter pillars, and to a smaller extent, those for a diameter of 1 μm, exhibited sizeable stochastic scatter. This may be attributed to the small testing loads: in the extreme case, i.e., for Ta pillars tested at 200 °C, loads as low as 100 μN were required for yielding, relatively close to the instrumental noise level (15 μN). This noise level caused an uncertainty of about 70 MPa in the extreme case (Ta pillars of 500 nm in diameter compressed at 200 °C). Still, the smallest load drops were noticeably above the instrumental noise. Their amplitude increased with increasing test temperature, indicating that larger dislocation avalanche events occurred at higher temperatures. For comparison, Figs. 3d and 4d show representative stress–strain curves of the largest and smallest micropillars for both Ta and W samples compressed at different temperatures. It can be observed that flow stresses scaled with pillar diameter for both Ta and W samples, and above all, that flow stresses were altered greatly by the test temperature. Furthermore, flow stress data converged for small pillars, implying that small pillars were less susceptible to temperature conditions.

Some W micropillars showed a stress maximum between 1 and 2% total strain, mostly the largest pillars compressed at room temperature (see Fig. 4a). This peak was followed by stress relaxation at small strains and has been previously attributed to contact misalignment between the flat punch and the top surface of micropillars as well as a slight geometrical tilt of the pillars [52]. This maximum can obscure the estimation of the yield point and subsequent determination of size effects as discussed later.

Observing Figs. 3 and 4, it is clear that the apparent strain hardening behavior was size dependent. It increased with decreasing diameter as previously reported in other BCC studies [22,23,27,28,32]. This was quantified in Fig. 5, which shows apparent strain hardening rate (SHR) as a function of pillar diameter at the different test temperatures. The SHR was determined as the slope in stress between 2 and 5% strain. Despite the significant scatter, a general trend was observed, where SHR values decreased with increasing temperature as opposed to what is observed for bulk BCC metals [53]. The W pillars generally showed a higher size dependence in the SHR than the Ta pillars, and the SHR values of W micropillars compressed at room temperature are consistent with previous room temperature W pillar studies [23]. In addition, the difference in SHR values as a function of temperature was larger for the W pillars than for the Ta pillars.

### 3.3. Dependence of size effect on yield criterion and temperature

In contrast to bulk compression tests, where the yield stress is usually defined as the stress at 0.2% plastic strain, the yield stress for micropillars is commonly determined by the stress at a given total strain value, typically between 2 and 10% [33]. This is done in order to minimize errors due to the initial stiffness artifacts and to ensure that the stress considered as the yield stress is beyond the first observed yield event, but not affected by strain hardening [14]. Here, the yield stress was carefully evaluated given the stochastic nature of the stress–strain curves and the noise shown by the compression system, which hindered the accurate determination of the yield stress.

The size effect on the strength of Ta and W micropillars is summarized in Fig. 6. The considered flow stress values were taken directly from the data at a certain strain level regardless of the stochastic behavior of the smallest pillars. By plotting the flow stress and the micropillar diameter on a log–log scale, power-law exponents were determined for the linear fit, as shown in Fig. 6a for both Ta and W samples at a total strain of 2.5% and at different temperatures. The stresses at 2.5% total strain were chosen in agreement with previous BCC micropillar studies [23,28,54]. This figure shows

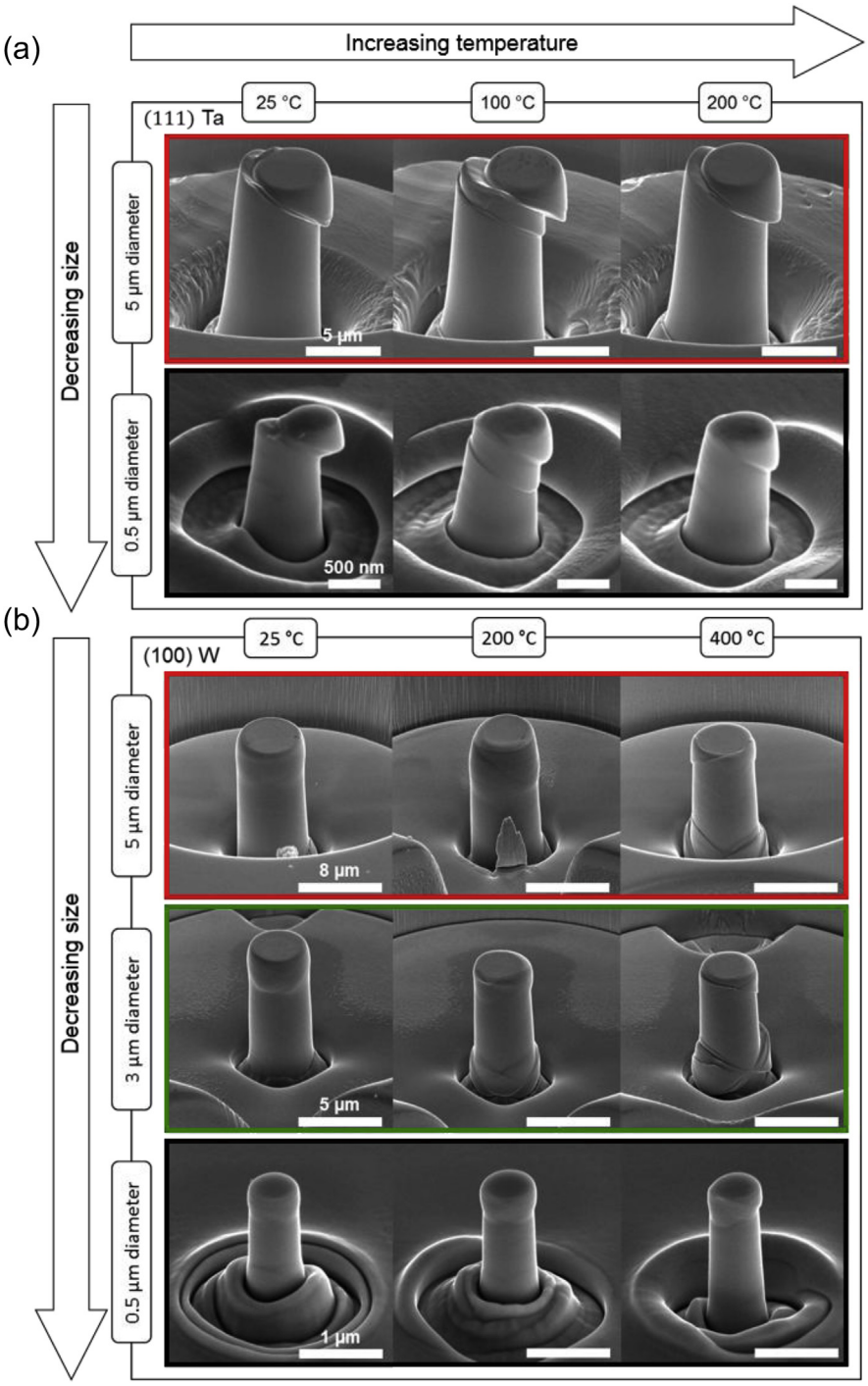


**Fig. 1.** Scanning electron microscopy images of representative micropillars after testing: (a) [111]-oriented Ta, with diameters of 5 and 0.5 µm compressed at 25, 100 or 200 °C, and (b) [100]-oriented W, with diameters of 5, 3 and 0.5 µm compressed at 25, 200 or 400 °C.

that flow stresses scaled inversely with the pillar diameter for both Ta and W samples, and more importantly, that test temperature had a significant influence on flow stress as also seen in high temperature nanoindentation measurements [55,56]. Interestingly, the data for Ta and W converged for small pillars, indicating that small pillars were less sensitive to temperature conditions as also reported by Schneider et al. [23]. Moreover, the room temperature flow stresses shown by both samples were consistent with previously reported data for W and Ta pillars [23,32].

For comparison, the power-law exponent was also calculated as a function of yield criterion, i.e., as a function of defined strain level. This was achieved by taking the stress values at different discrete strain values (every 0.025% strain) from 1 to 8% strain, and calculating, for each strain and respective stress levels, the power-law exponent as shown for 2.5% strain in Fig. 6a. Fig. 6b and c depict the power-law exponents for the Ta and W samples. For W, the power-law exponents are shown for a strain range between 1 and 8% at different temperatures, while for Ta, only

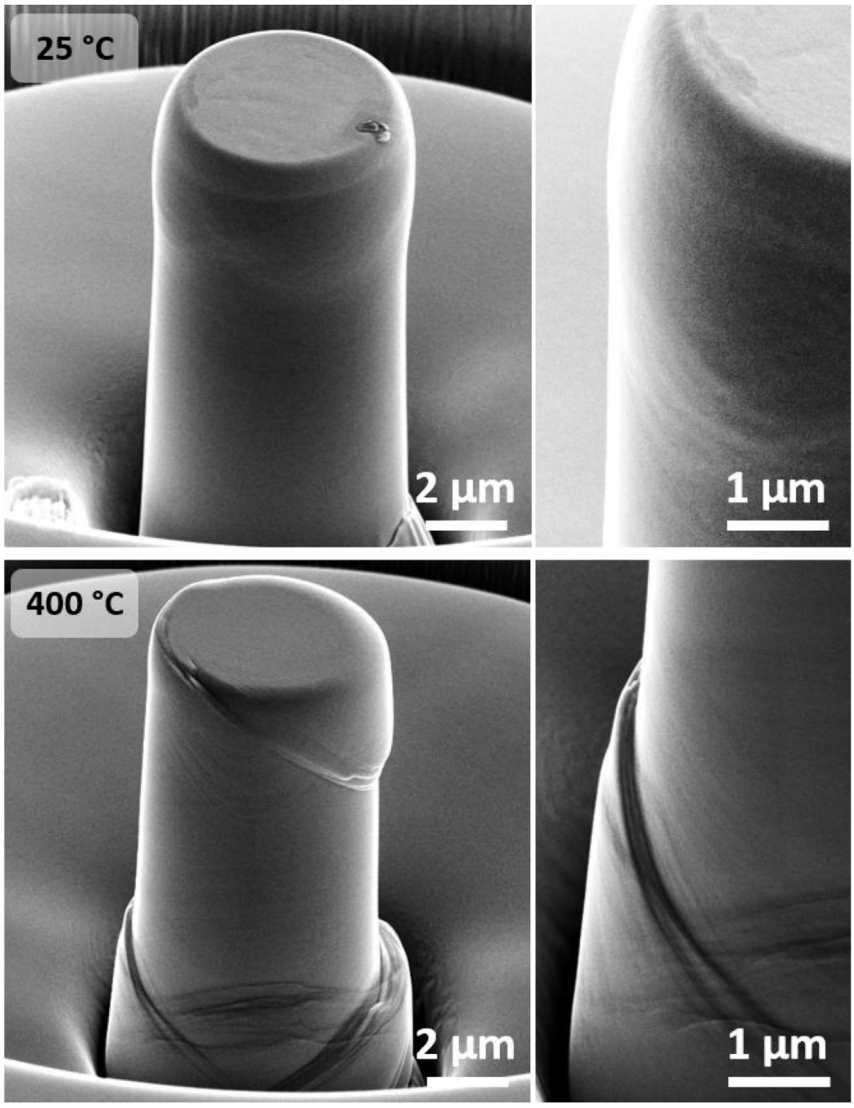


**Fig. 2.** Scanning electron microscopy images of two representative [100]-oriented W pillars with a diameter of 5 µm compressed at 25 and 400 °C. High resolution insets emphasize a change in deformation morphology with increasing test temperature: from homogeneous to localized deformation.

data between 1 and 5% are depicted as the larger Ta pillars were only deformed to a maximum strain of approximately 5% (see Fig. 3b). The power-law exponents determined in this way exhibited a general tendency despite of the inherent stochastic behavior of the stress–strain curves. For both samples, the exponents remained fairly constant at 25 °C with increasing strain while at higher temperatures, the exponents increased with increasing strain. An averaged power-law exponent between total strain values of 2 and 5% was determined at each temperature as most BCC studies on size effects have used different strain levels ranging between 2 and 5% [21–23,28,29,32,43,54]. Data below 2% total strain were not considered because these were influenced by the elastic behavior of the micropillars and the stress peaks described above. The resulting deviations at low strains are particularly observed in Fig. 6c for W micropillars.

As seen in Table 1, the averaged power-law exponents $n$ are – 0.37 ± 0.04, - 0.64 ± 0.06 and – 0.76 ± 0.07 for the Ta micropillars tested at 25, 100 and 200 °C and – 0.30 ± 0.01, - 0.46 ± 0.05 and – 0.60 ± 0.05 for the W micropillars tested at 25, 200 and 400 °C. A clear trend is observed that, with increasing temperature, the exponent increased in magnitude, reaching values that are in the range of previous FCC micropillar studies, i. e., –0.6 [10,11,14,33,57]. The results obtained at room temperature for both Ta and W micropillars were in close agreement with the literature [22,32].

## 4. Discussion

### *4.1. Effect of temperature on the deformation morphology of BCC pillars*

In the present study, Ta and W micropillars have, for the first time, been compressed at elevated temperatures. Ta micropillars were compressed at relatively large temperature ratios (test temperature/critical temperature between 0.66 and 1.05). Previous studies have shown two distinct deformation behaviors in BCC micropillars: a more localized slip deformation produced by the activation of a few slip systems, typically observed in BCC metals with low $T_c$ (such as Ta), and a more uniform deformation (wavy slip) related to the cross-slip of screw dislocations, seen in BCC metals with a high $T_c$ (such as W) [22]. These two different behaviors have been attributed to the temperature ratio, which, in turn, controls the mobility of screw dislocations. In view of this hypothesis, it is expected that, in our Ta micropillars, screw dislocations were relatively mobile. Hence, dislocations were mainly of mixed character and limited to

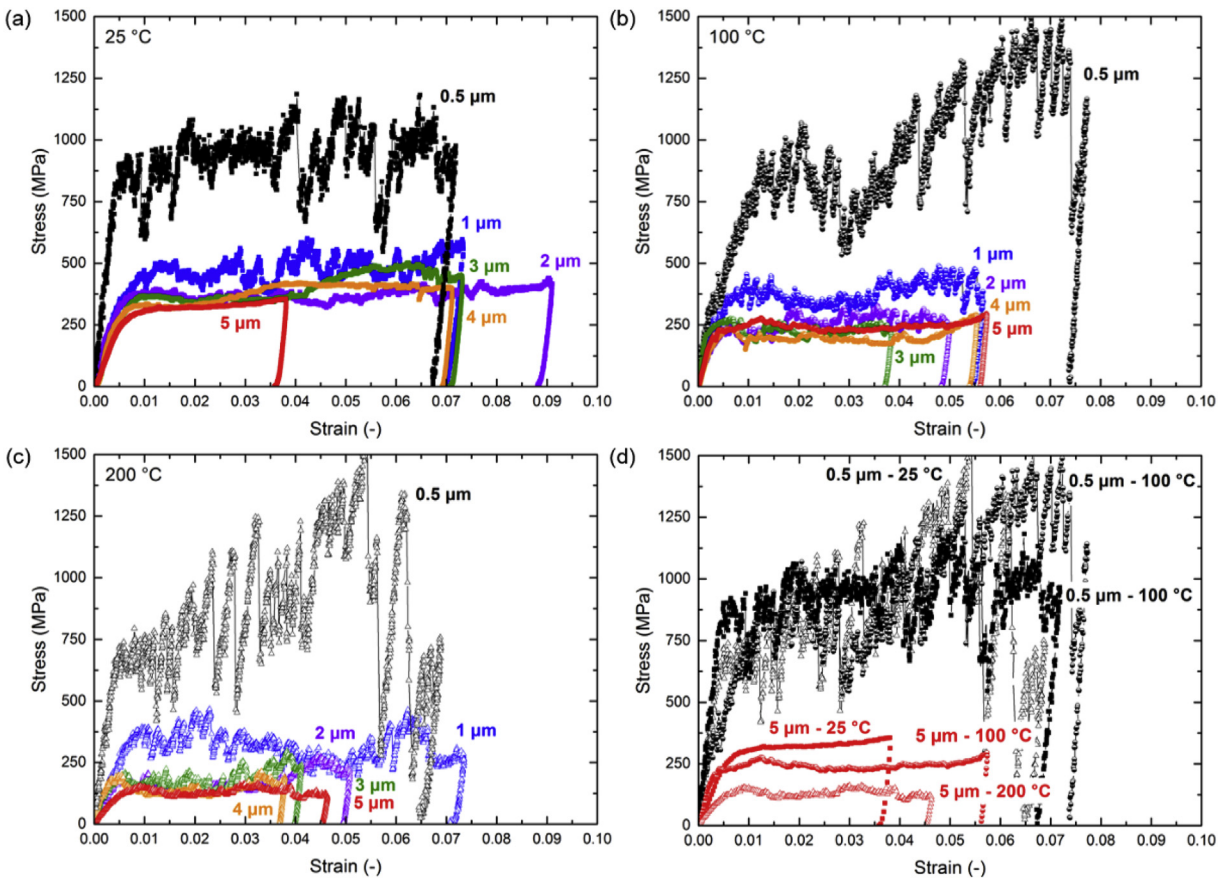


**Fig. 3.** Typical compressive stress–strain curves of different Ta micropillars with diameters ranging from 0.5 to 5 µm tested at different temperatures, (a) 25 °C, (b) 100 °C and (c) 200 °C. (d) Comparison of stress–strain curves for micropillars of 0.5 and 5 µm diameter taken from (a), (b) and (c). Squared solid symbols represent micropillar tests performed at 25 °C while triangular open symbols depict tests performed at 200 °C and circular semi-open symbols at 100 °C.

specific slip planes. As a result of this confinement, localized slip was observed [22].

For W pillars, the elevated temperature tests shed light, for the first time, on a temperature-dependent change of deformation morphology from uniform deformation to localized deformation (see Figs. 1 and 2). This indicates that, indeed, the temperature ratio has a strong influence on the motion of dislocations. At temperature ratios close to 1, screw and edge dislocations have comparable mobility due to the thermal activation. Thus, mixed dislocations are bound to particular slip planes [22]. As a consequence, large pillars compressed at high enough temperatures show localized slip. As $T_{test}/T_c$ decreases, screw dislocations become less mobile, and thus edge dislocations move faster toward the free surface of the micropillar, leaving the pillar in an edge dislocation-starved situation. Long and straight screw dislocation segments then lead the deformation via their ability to cross-slip between crystallographic planes which intersect along the <111> direction and cause a more uniform deformation of the pillar. In this respect, no transition from uniform to localized deformation is observed for the smallest W pillars with increasing temperature because the annihilation distance for edge dislocations will be shorter than for bigger pillars. Therefore, the pillars become edge-starved faster, so that the deformation is mainly controlled by the cross-slip of screw dislocations. This is in agreement with Fig. 1, where uniform wavy slip is observed for 500 nm pillars regardless of test temperature. In addition, it has been proposed that the motion of screw dislocations may be enhanced by the increase of surface-to-volume ratio with decreasing pillar size [21,32]. The explanation given is that edge dislocations near the free surface may assist kink nucleation and hence improve the mobility of screw dislocations [32]. Thus, the lattice resistance would be more easily overcome and the strength for small micropillars would not necessarily increase with decreasing pillar size. Also, at the submicron scale, the deformation is believed to be dominated by dislocation surface nucleation [58]. Thus, the strength size dependence of nanopillars would be expected to be weaker [59]. This is observed for 500 nm diameter W pillars in Fig. 6a, where a plateau in flow stress values is observed as the size decreases, i.e., flow stress values barely increase below 1 µm pillar diameter. The fact that the lattice resistance is more easily overcome at this size could also explain why the Ta and W pillars tested at different temperatures have the same strength.

### *4.2. Influence of yield criterion on size effects: effect of strain hardening on size effects*

As can be seen in Fig. 5, the SHR increases with decreasing sample size, as also observed for FCC and BCC micropillars compressed at room temperature [14,23,60]. This is in agreement with another BCC study of micropillar compressions performed at room temperature which has proposed that dislocation multiplication and related forest hardening are not the main factors for the strain hardening behavior as also observed for bulk BCC metals at temperatures well below $T_c$ [53,54]. It has been observed that pre-straining of Mo micropillars does not influence their hardening behavior [54]. Moreover, the 'reset' of their mechanical properties after repeated FIB machining suggests that their deformation is controlled by dislocation sources, i.e., defects caused by the ion cutting procedure. The strain hardening dependence of micropillars has been related to the

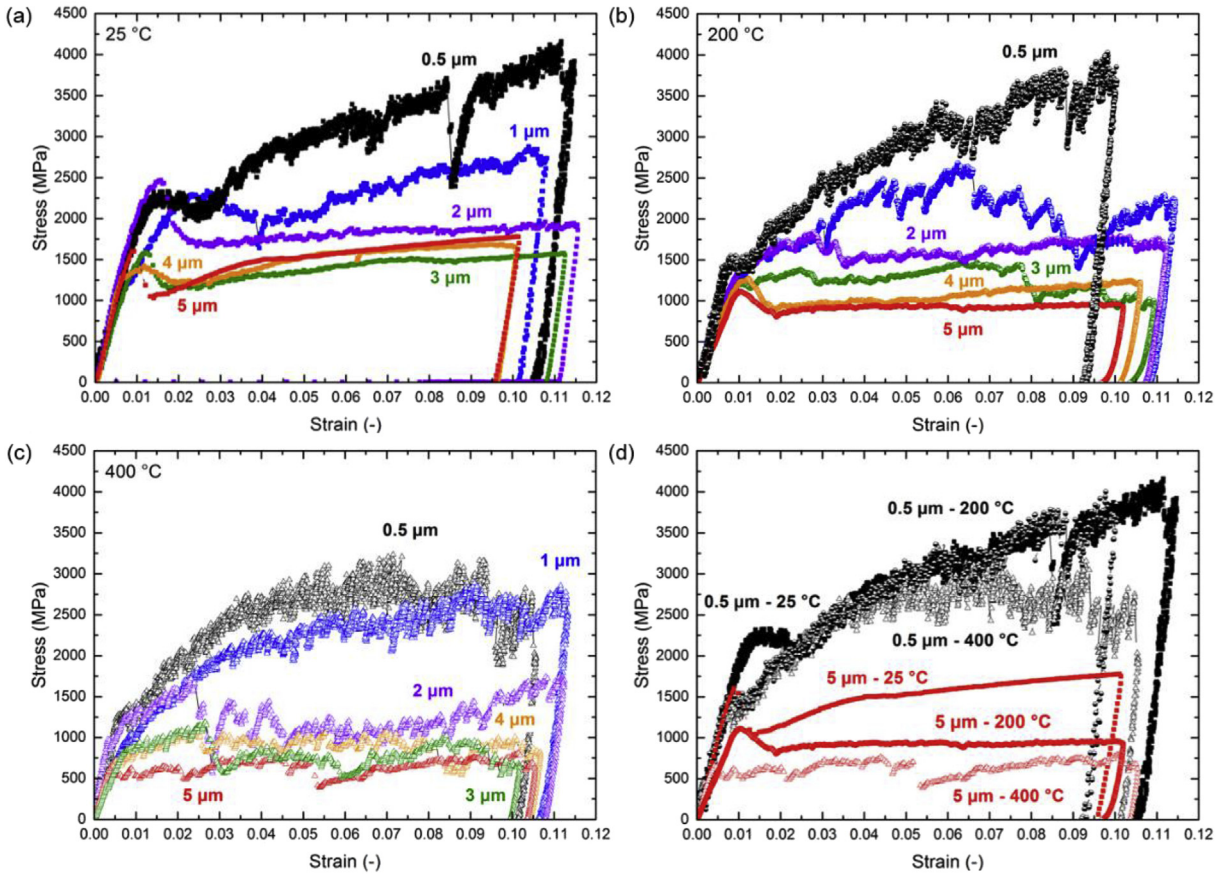


**Fig. 4.** Typical compressive stress–strain curves of different W micropillars with diameters ranging from 0.5 to 5 µm tested at different temperatures, (a) 25 °C, (b) 200 °C and (c) 400 °C. (d) Comparison of stress–strain curves for micropillars of 0.5 and 5 µm diameter taken from (a), (b) and (c). Squared solid symbols represent micropillar tests performed at 25 °C while triangular open symbols depict tests performed at 400 °C and circular semi-open symbols at 200 °C.

same mechanism as observed in FCC micropillars, i.e., exhaustion hardening, where the consumption of the weakest dislocation sources increases the stress needed to activate another dislocation source [14,45]. Nevertheless, this size dependence may be an artifact stemming from the pillar taper angle, which varies slightly as a function of pillar size. Although the Ta micropillars show some correlation between pillar taper as a function of diameter and SHR, the W micropillars clearly exhibit no direct correlation between these two parameters. Thus, this suggests that pillar taper does not account for such a strong size dependence.

More importantly, Fig. 5 shows that, for both Ta and W, the strain hardening behavior also depends on test temperature: lower SHRs are observed at higher temperatures. However, this temperature effect is opposed to bulk BCC metals, where the easier mobility of screw dislocations at higher temperatures increases dislocation forest hardening [53]. This different trend may be explained by the stress needed to activate a dislocation source, which can be approximated as being composed of an athermal nucleation stress, given by the nucleation barrier $Q^*$ and activation volume $V$, and a thermal stress [59]:

$$\sigma = \frac{Q^*}{V} - \frac{kT}{V} ln \frac{kTNv_0}{E\dot{\varepsilon}V}. \quad (3)$$

The latter term is characterized by a ratio between the thermal energy ($k{\cdot}T$) and $V$, given by the Boltzmann's constant $k$ and absolute temperature $T$, as well as a logarithmic function based on the competition between the thermal ($k{\cdot}T{\cdot}N{\cdot}v_0$) and mechanical ($E{\cdot}\dot{\varepsilon}{\cdot}V$) parameters. $N$ is the number of equivalent nucleation sites, $v_0$ the nucleation rate, $E$ the Young's modulus, and $\dot{\varepsilon}$ the strain rate. Assuming a relatively small $V$, in the range of 1–9 $b^3$ (characteristic of BCC micropillars compressed at similar strain rates) [61], and considering an elastic strain rate in the order of $5{\cdot}10^{-4}$ $s^{-1}$, an increase in the test temperature would be expected to decrease the nucleation stress. This was also suggested by atomistic simulations of surface dislocation nucleation [59]. A consequence will be a lower strain hardening as seen in Figs. 3–5. Moreover, the increase in strain hardening rate with decreasing sample size would explain the trend shown in the power-law exponent–strain curves in Fig. 6b and c, where a slight increment in the power-law exponent is observed as a function of increasing strain.

### 4.3. Size effects as a function of temperature

The present results indicate that the deformation mechanisms of submicron and micron-sized FIB machined BCC pillars depend on size as well as on temperature. In addition to an increase in yield strength with decreasing pillar diameter, both Ta and W pillars show lower yield strengths with increasing temperature (given a pillar diameter), as observed by Schneider et al. [21] for Mo only. This combined size and temperature dependence of strength of W and Ta micropillars can be assessed in terms of the different strengthening mechanisms as proposed by Parthasarathy et al. [46] (see Eq. (2)).

The strength is assumed to be the sum of a size independent bulk contribution and a size dependent contribution. For the latter, the statistical average length of the weakest single-arm dislocation

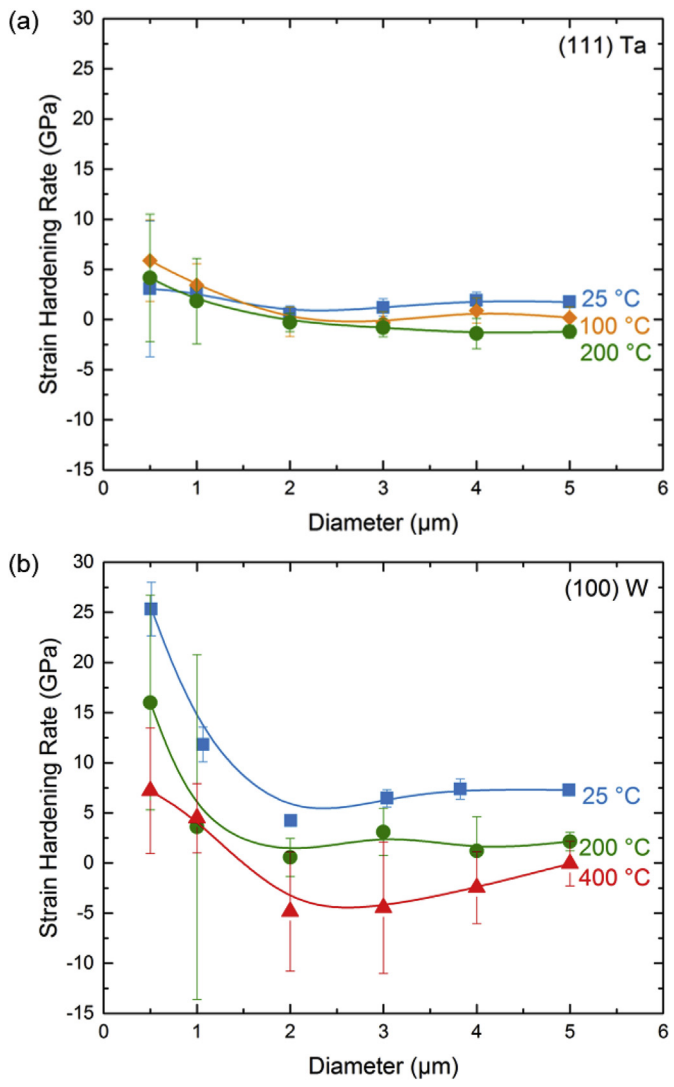


**Fig. 5.** Temperature dependence of the apparent strain hardening rate in (a) Ta and (b) W as a function of pillar diameter. The blue squares correspond to the average strain hardening rate (SHR) at 25 °C while the orange diamonds correspond to the averaged SHR at 100 °C, the green circles to the averaged SHR at 200 °C and the red triangles to the averaged SHR at 400 °C. Error bars illustrate the standard deviations in the measured SHR. (For interpretation of the references to color in this figure legend, the reader is referred to the web version of this article.)

source, $\bar{\lambda}_{max}$, must be calculated as the probability that a certain pillar with a diameter $d$, number $p$ of dislocation sources and a primary slip plane oriented at an angle $\beta$ to the compression axis has $\lambda_{max}$ as the maximum source length [46]:

$$\bar{\lambda}_{max} = \int_0^{d/2} \left[ 1 - \frac{4\left(\frac{d}{2} - \lambda_{max}\right)\left(\frac{d}{2\cos\beta} - \lambda_{max}\right)}{\frac{d^2}{\cos\beta}} \right]^{p-1} \cdot \left\{ \frac{4\left[\left(\frac{d}{2} - \lambda_{max}\right) + \left(\frac{d}{2\cos\beta} - \lambda_{max}\right)\right]}{\frac{d^2}{\cos\beta}} \right\} p\lambda_{max} d\lambda_{max}. \quad (4)$$

The number of sources, $p$, depends on the pillar dimensions (diameter $d$ and height $h$) and initial mobile dislocation density $\rho_{mob}$ as follows [46]:

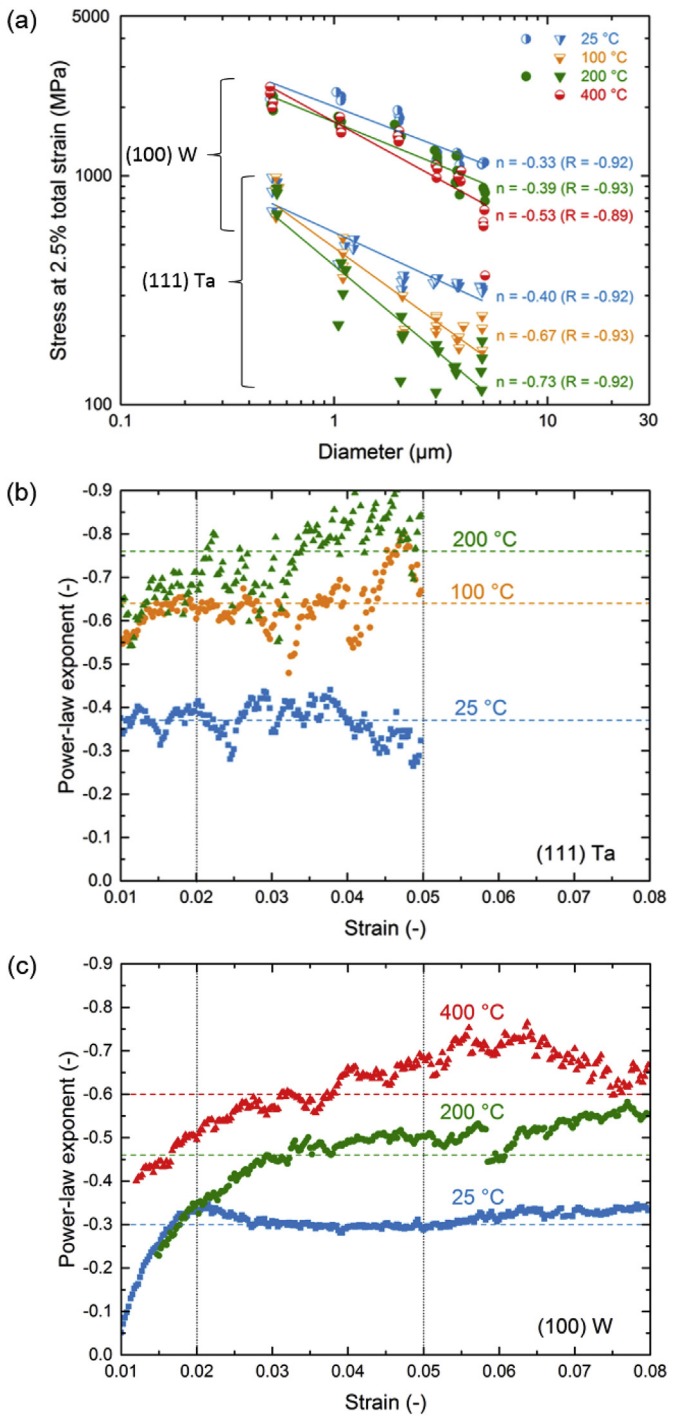


**Fig. 6.** Temperature dependence of the size effect in Ta and W: (a) Log–log plot of the flow stress taken at 2.5% total strain as a function of the top diameter of the W and Ta micropillars in the temperature range 25–400 °C. The solid lines depict best fit power-law functions. Influence of the yield criterion (strain) on the power-law exponent, $n$, at different temperatures for Ta (b) and W (c). The dashed horizontal lines in (b) and (c) correspond to the average $n$ values listed in Table 1 while the dotted vertical lines correspond to the lower and upper strain bounds of the average $n$ values.

$$p = Integer\left[\rho_{mob}\frac{\pi(d/2)^2 h}{L_{seg}}\right] = Integer\left[\frac{\pi\rho_{tot}(d/2)h}{s}\right], \quad (5)$$

where $L_{seg}$ is the average length of dislocation segments in the pillar, considered to be the pillar radius, and $s$ is the number of primary

**Table 1**
Temperature conditions and averaged power-law exponents *n* obtained from 2 to 5% total strain results presented in Fig. 6b and c. Critical temperatures taken from Ref. [22].

| | Temperature $T_{test}$ (°C, K) | Melting temperature $T_{melt}$ (°C, K) | Critical temperature $T_c$ (°C, K) | $T_{test}/T_c$ | $T_{test}/T_{melt}$ | 2–5% averaged total strain power-law exponent *n* |
|---|---|---|---|---|---|---|
| (111) Ta | 25 (298 K) | 3017 (3290 K) | 177 (450 K) | 0.66 | 0.09 | –0.37 ± 0.04 |
| | 100 (373 K) | | | 0.83 | 0.11 | –0.64 ± 0.06 |
| | 200 (473 K) | | | 1.05 | 0.14 | –0.76 ± 0.07 |
| (100) W | 25 (298 K) | 3422 (3695 K) | 527 (800 K) | 0.37 | 0.08 | –0.30 ± 0.01 |
| | 200 (473 K) | | | 0.59 | 0.13 | –0.46 ± 0.05 |
| | 400 (673 K) | | | 0.84 | 0.18 | –0.60 ± 0.05 |

slip systems, which is 12 for BCC metals ({112} <111> [38]). FIB machined micropillars are non-defect free, so that it is assumed that the current Ta and W micropillars have a moderate total dislocation density, $\rho_{tot}$, characteristic of annealed single crystals, i.e., $10^{10}$–$10^{13}$ $m^{-2}$ [42,46]. The dislocation density for both materials is assumed to be stable in the tested temperature range as temperature induced dislocation annealing, i.e., recovery, can be neglected at these low homologous temperatures (see Table 1).

The material parameters needed to evaluate the equation by Parthasarathy et al. are presented in Table 2. The lattice resistance values, $\tau_0$, of Ta at different temperatures were taken from Smialek et al. [62], who tested single slip oriented Ta single crystals at different temperatures at similar strain rates as in the present study. For W, no lattice resistance values are available for [100]-oriented single crystals in compression. However, data taken from Brunner [63], who performed tensile tests of W crystals up to 800 K, were used as a first approach. The temperature-dependent values of the shear moduli of [111]-oriented Ta and [100]-oriented W single crystals were taken from two different studies [64,65]. The weak temperature dependence of the Burgers' vector was neglected.

The yield stresses calculated from eqs. (2), (4) and (5) as a function of size and temperature are shown in Fig. 7. The predicted results for Ta agree very well with the experimental data. For W micropillars, the agreement between experimental and theoretical values is not as good as for the Ta pillars (Fig. 7b): the experimental yield stress values are much less dependent on temperature than the calculated values; there are also indications that the size dependence is weaker than predicted. The predicted values generally come to lie below the experimental ones. While the assumed lattice friction stresses affect mainly the absolute level of the predicted yield stresses, the dislocation density strongly affects the size dependence. Lee and Nix [42] suggested that an increase in the dislocation density would affect the yield stress of pillars differently depending on their size: weakening for submicron-sized pillars and hardening for micron-sized pillars. Higher dislocation densities would then decrease the size effect as observed in Fig. 7b and also by Lee and Nix [42]. This would also decrease the temperature dependence of the yield stresses as seen in Fig. 7b. However, this does not explain yet the different sign of curvature shown by the W experimental data, suggesting that other strengthening factors may govern the plastic deformation of W micropillars. For instance, the effective stress needed to yield might be affected by the enhancement of the screw dislocation mobility due to kink nucleation at the pillar surface [23,66]. Due to the larger surface to volume ratio, the lattice resistance would be more easily overcome with decreasing pillar size. Thus, less mechanical work than expected would be needed to overcome the lattice friction for the small W pillars. The fact that the lattice friction values of Ta are close to zero at the current temperature regime might explain why the model works well for Ta, while for W, with larger lattice friction values, the model does not follow the experimental trend. In addition, this might also explain why the W pillars are less sensitive to temperature changes as sample size decreases.

The different power-law exponents shown by the Ta and W micropillars can be correlated with the relative test temperature, i.e., $T_{test}/T_c$, as first shown by Schneider et al. [22]. The lattice resistance strongly depends on $T_{test}/T_c$ for BCC metals [67]. Thus, it is expected that size effects scale with this relative test temperature [22]. Fig. 8 provides an overall view of power-law exponents as a function of this temperature ratio. The average experimental power-law exponents of Ta and W micropillars shown in Table 1 for the current study are depicted (closed symbols) together with a schematic of the different exponents observed for other BCC metals [21–23,32,54,68]. In addition, the power-law exponents for Ta and W micropillars predicted by the model of Parthasarathy et al. are presented (open symbols). As observed in Fig. 8, the power-law exponents of the Ta and W micropillars decrease with increasing relative test temperature as was previously reported for Mo [21,22]. It is emphasized that the present results fit well into the overall picture: for relative temperatures approaching 1 (for W: 400 °C, Ta: 200 °C), a size dependence typical for FCC micropillars [10,14], with $n \leq -0.6$, is found. The pillars tested at higher temperatures show a more negative exponent, i.e., a more pronounced size effect, which indicates that the size-independent terms in eq. (2) lose in relative importance. This could be explained, for example, by a progressive decrease in the lattice resistance. On the defect level, this behavior can be attributed, as suggested previously [21], to the important role of screw dislocations: as their mobility increases with rising temperature, especially when the critical temperature is exceeded, the deformation approaches that of FCC metals.

Also, the experimental power-law exponents of Ta agree reasonably well with the exponents predicted using the single-arm dislocation source model. However, the predicted power-law exponents of the W micropillars compressed at 400 °C are much lower than the experimental ones. The fact that the predicted yield stresses calculated as a function of the pillar diameter do not capture the

**Table 2**
Material parameters of Ta and W at different temperatures.

| Material | Temperature (°C) | Schmid factor *m* | $\tau_0$ (MPa) | μ (GPa) | b (Å) | β (°) – slip plane orientation |
|---|---|---|---|---|---|---|
| Ta | 25 | 0.314 | 45 [62] | 69 [64] | 2.860 | 19.5 |
| | 100 | | 15 [62] | 68 [64] | | |
| | 200 | | ~0 | 67.4 [64] | | |
| W | 25 | 0.471 | 384 [63] | 159 [65] | 2.741 | 35.3 |
| | 200 | | 213 [63] | 156 [65] | | |
| | 400 | | 48 [63] | 152 [65] | | |

Lattice resistance in shear, $\tau_0$, of Ta from Ref. [62], and $\tau_0$s of W from Ref. [63]. Corresponding shear moduli, $\mu$, of W from Ref. [65] and of Ta from Ref. [64].

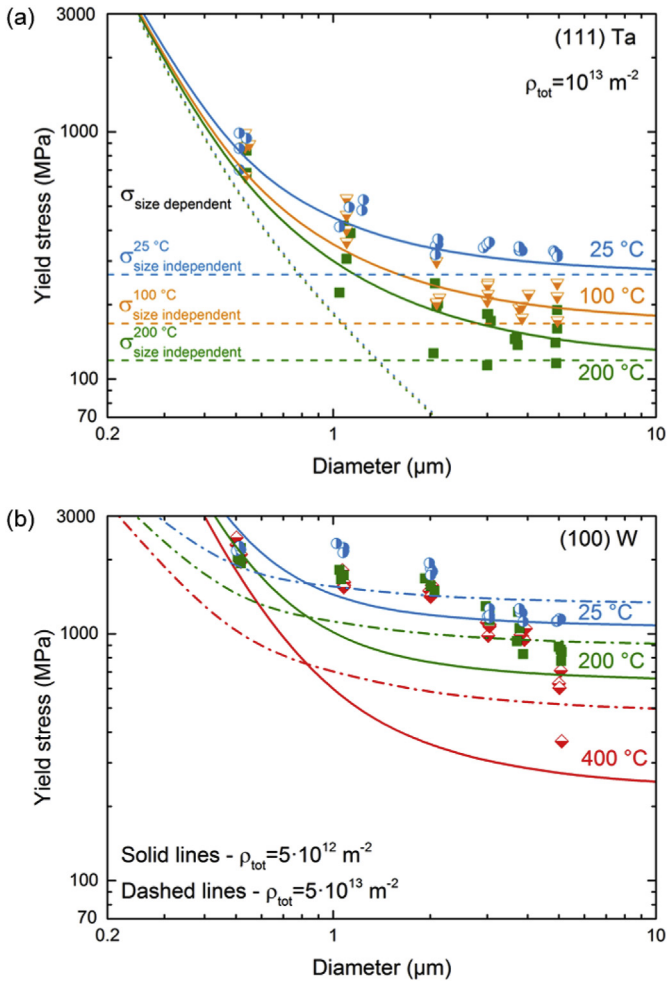


**Fig. 7.** Comparison between experimental yield stresses determined at 2.5% total strain and calculated ones using the model by Parthasarathy et al. (Eqs. (2), (4) and (5)) of (a) Ta micropillars compressed at 25, 100 and 200 °C and (b) W micropillars tested at 25, 200 and 400 °C. In (a), the solid lines represent the predicted yield stresses as a function of pillar diameter, assuming a dislocation density of $10^{13}$ m$^{-2}$. The dashed and dotted lines correspond to the size independent and size dependent contributions to the yield stresses, respectively. In (b), the solid lines correspond to the predicted yield stresses assuming a dislocation density of $5{\cdot}10^{12}$ m$^{-2}$ while the dashed-dotted lines correspond to an alternative calculation with a dislocation density of $5\times10^{13}$ m$^{-2}$.

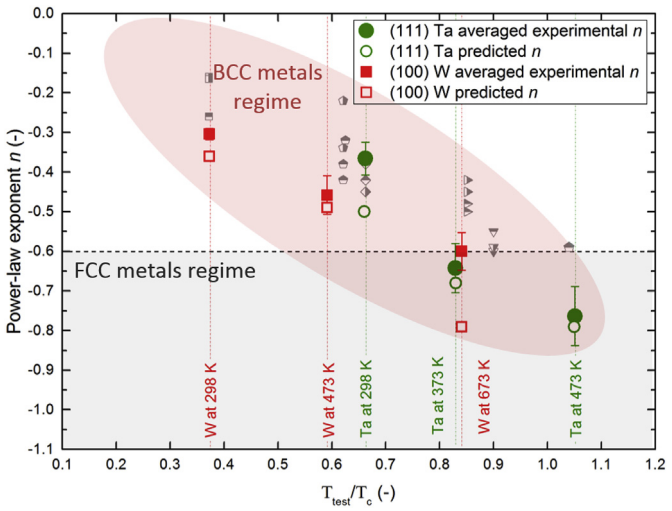


**Fig. 8.** Power-law exponent $n$ as a function of the relative test temperature $T_{test}/T_c$. The solid symbols represent the experimental results of this work while the open symbols depict the theoretical prediction of $n$ calculated according to the model by Parthasarathy et al. Included for comparison are different size effects of BCC micropillars determined in other studies [21,22,32,68].

experimental trend produces such overestimation of the size effects. As discussed above, the actual W micropillars may have larger initial dislocation density and lattice resistance values than the ones used for the estimation, which together with other strengthening mechanisms, may produce this disparity. Nevertheless, it is apparent that the initial dislocation density and temperature dependence of the lattice friction play an important role in determining the size dependence on strength of micropillars. Assuming a constant initial dislocation density with increasing temperature, the lattice resistance dictates the size effect of BCC micropillars as a function of temperature.

In order to arrive at a better estimate of the different strengthening mechanisms and to go beyond this study, knowledge of the initial dislocation density of the pillars would be helpful. Moreover, the determination of the exact lattice resistance of the samples as a function of temperature would be of significant importance since it has been observed that it plays a crucial role in the deformation of BCC micropillars. Also, questions arise regarding the emergence of plastic flow and evolution of plasticity (strain hardening) in BCC micropillars and its temperature dependence, which are directly related to the activation of single-arm dislocation sources, surface dislocation annihilation, dislocation storage and consequent dislocation interactions. Therefore, *in situ* transmission electron microscopy compression experiments as well as computational simulations would give further fundamental information to the understanding of BCC plasticity confined in micron-sized samples as a function of temperature.

## 5. Conclusion

For the first time, elevated temperature compression tests were carried out on [111]-oriented Ta and [100]-oriented W pillars with diameters of a few micrometers in order to study the influence of temperature on the size effect. The following conclusions can be drawn:

- The temperature ratio ($T_{test}/T_c$) has a strong influence on the relative motion of screw and edge dislocations. Slip traces characteristic of localized single slip were observed on the surfaces of the tested Ta pillars irrespective of test temperature. In W pillars, a change from uniform wavy deformation to localized deformation was observed with increasing temperature and pillar size.
- The stress–strain behavior became more stochastic as the pillar size decreased, and their plastic intermittencies (load drops) were altered by the amount of thermal energy provided: at higher temperatures, plastic intermittency was qualitatively larger.
- The apparent strain hardening behavior was not only size dependent but, more importantly, test temperature dependent. Despite significant experimental scatter, strain hardening was clearly found to decrease with increasing temperature. This effect was attributed to easier activation of dislocation sources near the surface and better dislocation mobility at higher temperatures.
- Both materials exhibited larger size effects at higher temperatures. The size dependence scaled with the ratio of test temperature to critical temperature. For test temperatures close to or larger than $T_c$, FCC size dependence was reached.
- The contributions of bulk strength and size-dependent stresses to size effects at different temperatures were analyzed by using

the single-arm dislocation source model. While the model reproduced the Ta results very well, it could not capture the experimental trend shown by the W micropillars. Assuming a constant initial dislocation density, the temperature-dependent size effects of BCC micropillars depend mainly on the magnitude of the lattice resistance ($T_{test}/T_c$).

By reporting microcompression tests at elevated temperatures, this work provides new evidence on the effect of temperature on the plasticity of micron-sized BCC samples as well as further insight into their deformation mechanisms. Such studies help to establish a basis for the design of BCC metal microstructures in high-temperature applications and to estimate material strength for a given sample dimension.

## Acknowledgments

The authors thank Prof. Dr. C. Motz from the Department of Materials Science and Methods, Saarland University (Saarbrücken, Germany), and Dr. A. Caron from the INM-Leibniz Institute for New Materials for valuable discussions about data analysis and interpretation. Also, thanks to Mr. B. Medina Clavijo for his assistance. E. A. acknowledges partial support through the European Union's Seventh Framework Program (FP/2007-2013)/ERC Advanced Grant Agreement No. 340929.

## References

[1] E. Arzt, Size effects in materials due to microstructural and dimensional constraints: a comparative review, Acta Mater 46 (1998) 5611–5626.
[2] J.R. Greer, J.T.M. De Hosson, Plasticity in small-sized metallic systems: Intrinsic versus extrinsic size effect, Prog. Mater. Sci. 56 (2011) 654–724.
[3] E.O. Hall, The deformation and ageing of mild steel: III Discussion of results, Proc. Phys. Soc. Sect. B 64 (1951) 747.
[4] N.J. Petch, The cleavage strength of polycrystals, Iron Steel Inst. 174 (1953) 25–28.
[5] N.A. Fleck, J.W. Hutchinson, Strain gradient plasticity, Adv. Appl. Mech. (1997) 295–361.
[6] W.D. Nix, H. Gao, Indentation size effects in crystalline materials: A law for strain gradient plasticity, J. Mech. Phys. Solids 46 (1998) 411–425.
[7] Y. Chen, O. Kraft, M. Walter, Size effects in thin coarse-grained gold microwires under tensile and torsional loading, Acta Mater 87 (2015) 78–85.
[8] M.D. Uchic, D.M. Dimiduk, J.N. Florando, W.D. Nix, Sample dimensions influence strength and crystal plasticity, Science 305 (2004) 986–989.
[9] Z.W. Shan, R.K. Mishra, S. A Syed Asif, O.L. Warren, A.M. Minor, Mechanical annealing and source-limited deformation in submicrometre-diameter Ni crystals, Nat. Mater 7 (2008) 115–119.
[10] D.M. Dimiduk, M.D. Uchic, T.A. Parthasarathy, Size-affected single-slip behavior of pure nickel microcrystals, Acta Mater 53 (2005) 4065–4077.
[11] C.P. Frick, B.G. Clark, S. Orso, A.S. Schneider, E. Arzt, Size effect on strength and strain hardening of small-scale [111] nickel compression pillars, Mater. Sci. Eng. A 489 (2008) 319–329.
[12] J. Greer, W. Nix, Nanoscale gold pillars strengthened through dislocation starvation, Phys. Rev. B 73 (2006) 245410.
[13] J.R. Greer, W.C. Oliver, W.D. Nix, Size dependence of mechanical properties of gold at the micron scale in the absence of strain gradients, Acta Mater 53 (2005) 1821–1830.
[14] C.A. Volkert, E.T. Lilleodden, Size effects in the deformation of sub-micron Au columns, Philos. Mag. 86 (2006) 5567–5579.
[15] J.-Y. Kim, J.R. Greer, Tensile and compressive behavior of gold and molybdenum single crystals at the nano-scale, Acta Mater 57 (2009) 5245–5253.
[16] J.R. Greer, C.R. Weinberger, W. Cai, Comparing the strength of f.c.c. and b.c.c. sub-micrometer pillars: compression experiments and dislocation dynamics simulations, Mater. Sci. Eng. A 493 (2008) 21–25.
[17] W.D. Nix, J.R. Greer, G. Feng, E.T. Lilleodden, Deformation at the nanometer and micrometer length scales: Effects of strain gradients and dislocation starvation, Thin Solid Films 515 (2007) 3152–3157.
[18] D. Kiener, C. Motz, T. Schöberl, M. Jenko, G. Dehm, Determination of mechanical properties of copper at the micron scale, Adv. Eng. Mater 8 (2006) 1119–1125.
[19] D. Kiener, A.M. Minor, Source-controlled yield and hardening of Cu (1 0 0) studied by in situ transmission electron microscopy, Acta Mater 59 (2011) 1328–1337.
[20] K.S. Ng, A.H.W. Ngan, Stochastic nature of plasticity of aluminum micro-pillars, Acta Mater 56 (2008) 1712–1720.
[21] A.S. Schneider, C.P. Frick, E. Arzt, W.J. Clegg, S. Korte, Influence of test temperature on the size effect in molybdenum small-scale compression pillars, Philos. Mag. Lett. (2013) 1–8.
[22] A.S. Schneider, D. Kaufmann, B. Clark, C. Frick, P. Gruber, R. Mönig, et al., Correlation between critical temperature and strength of small-scale bcc pillars, Phys. Rev. Lett. 103 (2009) 1–4.
[23] A.S. Schneider, C.P. Frick, B.G. Clark, P.A. Gruber, E. Arzt, Influence of orientation on the size effect in bcc pillars with different critical temperatures, Mater. Sci. Eng. A (2011) 1540–1547.
[24] S.-W. Lee, Y. Cheng, I. Ryu, J. Greer, Cold-temperature deformation of nano-sized tungsten and niobium as revealed by in-situ nano-mechanical experiments, Sci. China Technol. Sci. 57 (2014) 652–662.
[25] M. Zaiser, J. Schwerdtfeger, A.S. Schneider, C.P. Frick, B.G. Clark, P. A Gruber, et al., Strain bursts in plastically deforming molybdenum micro- and nanopillars, Philos. Mag. 88 (2008) 3861–3874.
[26] J.-Y. Kim, J.R. Greer, Size-dependent mechanical properties of molybdenum nanopillars, Appl. Phys. Lett. 93 (2008) 101913–101916.
[27] S. Brinckmann, J.-Y. Kim, J.R. Greer, Fundamental differences in mechanical behavior between two types of crystals at the nanoscale, Phys. Rev. Lett. 100 (2008) 155502.
[28] A.S. Schneider, B.G. Clark, C.P. Frick, P.A. Gruber, E. Arzt, Effect of orientation and loading rate on compression behavior of small-scale Mo pillars, Mater. Sci. Eng. A 508 (2009) 241–246.
[29] J.-Y. Kim, D. Jang, J.R. Greer, Tensile and compressive behavior of tungsten, molybdenum, tantalum and niobium at the nanoscale, Acta Mater 58 (2010) 2355–2363.
[30] J.-Y. Kim, D. Jang, J.R. Greer, Insight into the deformation behavior of niobium single crystals under uniaxial compression and tension at the nanoscale, Scr. Mater 61 (2009) 300–303.
[31] S.M. Han, T. Bozorg-Grayeli, J.R. Groves, W.D. Nix, Size effects on strength and plasticity of vanadium nanopillars, Scr. Mater 63 (2010) 1153–1156.
[32] D. Kaufmann, R. Mönig, C.A. Volkert, O. Kraft, Size dependent mechanical behaviour of tantalum, Int. J. Plast. 27 (2011) 470–478.
[33] M.D. Uchic, P.A. Shade, D.M. Dimiduk, Plasticity of micrometer-scale single crystals in compression, Annu. Rev. Mater. Res. 39 (2009) 361–386.
[34] M.D. Uchic, D.M. Dimiduk, A methodology to investigate size scale effects in crystalline plasticity using uniaxial compression testing, Mater. Sci. Eng. A 400–401 (2005) 268–278.
[35] M.D. Uchic, D.M. Dimiduk, R. Wheeler, P.A. Shade, H.L. Fraser, Application of micro-sample testing to study fundamental aspects of plastic flow, Scr. Mater 54 (2006) 759–764.
[36] D. Kiener, C. Motz, G. Dehm, Micro-compression testing: A critical discussion of experimental constraints, Mater. Sci. Eng. A 505 (2009) 79–87.
[37] V. Vitek, V. Paidar, Non-planar dislocation cores: A ubiquitous phenomenon affecting mechanical properties of crystalline materials, in: Dislocations in Solids, Elsevier, 2008, pp. 439–514.
[38] A. Seeger, Peierls barriers, kinks, and flow stress: recent progress, Int. J. Mater. Res. 93 (2002) 760–777.
[39] S. Korte, W.J. Clegg, Discussion of the dependence of the effect of size on the yield stress in hard materials studied by microcompression of MgO, Philos. Mag. 91 (2011) 1150–1162.
[40] D.E. Segall, A. Strachan, W.A. Goddard III, S. Ismail-Beigi, T.A. Arias, Ab initio and finite-temperature molecular dynamics studies of lattice resistance in tantalum, Phys. Rev. B 68 (2003) 14104.
[41] K.G. Hoge, A.K. Mukherjee, The temperature and strain rate dependence of the flow stress of tantalum, J. Mater. Sci. 12 (1977) 1666–1672.
[42] S.-W. Lee, W.D. Nix, Size dependence of the yield strength of fcc and bcc metallic micropillars with diameters of a few micrometers, Philos. Mag. 92 (2012) 1238–1260.
[43] J.-Y. Kim, D. Jang, J.R. Greer, Crystallographic orientation and size dependence of tension–compression asymmetry in molybdenum nano-pillars, Int. J. Plast. 28 (2012) 46–52.
[44] J.A. El-Awady, M.D. Uchic, P.A. Shade, S.-L. Kim, S.I. Rao, D.M. Dimiduk, et al., Pre-straining effects on the power-law scaling of size-dependent strengthening in Ni single crystals, Scr. Mater 68 (2013) 207–210.
[45] S.I. Rao, D.M. Dimiduk, T.A. Parthasarathy, M.D. Uchic, M. Tang, C. Woodward, Athermal mechanisms of size-dependent crystal flow gleaned from three-dimensional discrete dislocation simulations, Acta Mater 56 (2008) 3245–3259.
[46] T.A. Parthasarathy, S.I. Rao, D.M. Dimiduk, M.D. Uchic, D.R. Trinkle, Contribution to size effect of yield strength from the stochastics of dislocation source lengths in finite samples, Scr. Mater 56 (2007) 313–316.
[47] R. Soler, J.M. Wheeler, H.-J. Chang, J. Segurado, J. Michler, J. Llorca, et al., Understanding size effects on the strength of single crystals through high-temperature micropillar compression, Acta Mater 81 (2014) 50–57.
[48] J.M. Wheeler, J. Michler, Elevated temperature, nano-mechanical testing in situ in the scanning electron microscope, Rev. Sci. Instrum. 84 (2013) 45103–45115.
[49] J.M. Wheeler, C. Niederberger, C. Tessarek, S. Christiansen, J. Michler, Extraction of plasticity parameters of GaN with high temperature, in situ micro-compression, Int. J. Plast. 40 (2013) 140–151.
[50] I. Sneddon, The relation between load and penetration in the axisymmetric boussinesq problem for a punch of arbitrary profile, Int, J. Eng. Sci. 3 (1965) 47–57.
[51] K.S. Ng, A.H.W. Ngan, Stochastic theory for jerky deformation in small crystal volumes with pre-existing dislocations, Philos. Mag. 88 (2008) 677–688.
[52] R. Soler, J.M. Molina-Aldareguia, J. Segurado, J. LLorca, Effect of misorientation on the compression of highly anisotropic single-crystal micropillars, Adv. Eng. Mater 14 (2012) 1004–1008.
[53] B. Sesták, A. Seeger, Gleitung und Verfestigung in kubisch-raumzentrierten Metallen und Legierungen (I), Z. Met. 69 (1978) 195.

[54] A.S. Schneider, B.G. Clark, C.P. Frick, P.A. Gruber, E. Arzt, Effect of pre-straining on the size effect in molybdenum pillars, Philos. Mag. Lett. 90 (2010) 841–849.
[55] O. Franke, J. Alcalá, R. Dalmau, Z.C. Duan, J. Biener, M.M. Biener, et al., Incipient plasticity of single-crystal tantalum as a function of temperature and orientation, Philos. Mag. (2014) 1–12.
[56] J.S.K.-L. Gibson, S.G. Roberts, D.E.J. Armstrong, High temperature indentation of helium-implanted tungsten, Mater. Sci. Eng. A 625 (2015) 380–384.
[57] D. Kiener, C. Motz, M. Rester, M. Jenko, G. Dehm, FIB damage of Cu and possible consequences for miniaturized mechanical tests, Mater. Sci. Eng. A 459 (2007) 262–272.
[58] L.Y. Chen, M. He, J. Shin, G. Richter, D.S. Gianola, Measuring surface dislocation nucleation in defect-scarce nanostructures, Nat. Mater 14 (2015) 707–713.
[59] T. Zhu, J. Li, A. Samanta, A. Leach, K. Gall, Temperature and strain-rate dependence of surface dislocation nucleation, Phys. Rev. Lett. 100 (2008) 25502.
[60] D. Kiener, P.J. Guruprasad, S.M. Keralavarma, G. Dehm, A.A. Benzerga, Work hardening in micropillar compression: In situ experiments and modeling, Acta Mater 59 (2011) 3825–3840.
[61] A.S. Schneider, B.G. Clark, C.P. Frick, E. Arzt, Correlation between activation volume and pillar diameter for Mo and Nb bcc pillars, MRS Online Proc. Libr. 1185 (2009), 1185–II07–04.
[62] R.L. Smialek, G.L. Webb, T.E. Mitchell, Solid solution softening in bcc metal alloys, Scr. Metall. 4 (1970) 33–37.
[63] D. Brunner, Comparison of flow-stress measurements on high-purity tungsten single crystals with the kink-pair theory, Mater. Trans. JIM 41 (2000) 152–160.
[64] D. Orlikowski, P. Söderlind, J.A. Moriarty, First-principles thermoelasticity of transition metals at high pressure: Tantalum prototype in the quasiharmonic limit, Phys. Rev. B 74 (2006) 54109.
[65] R. Lowrie, M. Gonas, Single-crystal elastic properties of tungsten from 24 to 1800°C, J. Appl. Phys. 38 (1967) 4505.
[66] D. Kaufmann, A.S. Schneider, R. Mönig, C.A. Volkert, O. Kraft, Effect of surface orientation on the plasticity of small bcc metals, Int. J. Plast. 49 (2013) 145–151.
[67] A.S. Argon, Strengthening Mechanisms in Crystal Plasticity, Oxford University Press, Oxford; New York, 2008.
[68] B.R.S. Rogne, C. Thaulow, Strengthening mechanisms of iron micropillars, Philos. Mag (2014) 1–15.